

**MODELING OF A POSITION SERVO USED IN ROBOTICS APPLICATIONS**

MARCOS R. O. A. MAXIMO\*, CARLOS H. C. RIBEIRO\*, RUBENS J. M. AFONSO†

*\*Autonomous Computational Systems Lab (LAB-SCA), Computer Science Division, Aeronautics Institute of Technology, Praça Marechal Eduardo Gomes, 50, Vila das Acácias, 12228-900, São José dos Campos, SP, Brazil**†Electronic Engineering Division, Aeronautics Institute of Technology, Praça Marechal Eduardo Gomes, 50, Vila das Acácias, 12228-900, São José dos Campos, SP, Brazil*Emails: `mmaximo@ita.br`, `carlos@ita.br`, `rubensjm@ita.br`

**Abstract**— Position servos are extensively used as actuators for robots. In particular, Dynamixel servos from Robotis are employed as the actuator in each of the 20 joints of a humanoid research robot known as Darwin OP2. The lack of adequate dynamic modeling of the servo behavior renders control applications more difficult, as the performance of the control system is compromised due to model-plant mismatches. In the present paper we develop and validate experimentally a model for the behavior of the Dynamixel MX-28AT, including phenomena such as viscous friction and saturation. Such a model allows the correct simulation of the servo behavior and the adequate design of controllers.

**Keywords**— Modeling, Servo, Actuator.

## 1 Introduction

Servomechanisms are widely used as actuators in robotics applications (Gouaillier et al., 2009; Wensing et al., 2017; Zhao et al., 2015). Nonetheless, adequate models of the dynamics are frequently not available for many of the low-cost or hobby servos, compromising the capability of performing high fidelity simulations and readjusting the inner control loop of the servo, when possible, to achieve desired dynamic performance for the specific application.

In particular, modern servos such as the Dynamixel MX-28AT present interesting characteristics, such as a high torque per volume ratio, low dissipation, high communication bandwidth (ROBOTIS, 2010a), empowering many new high performance applications. Moreover, Dynamixel servos connections may be daisy-chained, greatly simplifying the wiring in the robot structure when many servos are used, such as in a humanoid robot. One of the examples is the open project humanoid robot ROBOTIS OP-2, also known as Darwin (Ha et al., 2011).

Nevertheless, no analytical model that adequately describes the dynamics of the robot is available in the Literature, rendering the transition between conceptual algorithms and control laws to practical experiments somewhat uncertain and trial and error based. It would, therefore, be an interesting enhancement both for academia as well as competitors to dispose of a high fidelity model for simulation. Other advantages of having an accurate model are the capability of performing many tests, such as required for learning-based algorithms for control and movement planning, testing more radical changes in the algorithms with no risk to the robot, thus enhancing the maturity of experiments with the real platform, and simu-

lating a high number of robots as in a team for robot soccer, since many groups lack the financial resources to acquire an entire team.

One first step in modeling the full body dynamics of the humanoid robot and also of other mechanisms employing the MX-28AT servo as actuators is to count with an accurate dynamical model of the servo itself, which is capable of encompassing all the effects that are relevant to the performance, including the order of the dynamics, the involved time constants and nonlinear phenomena, such as quantization and saturation. Moreover, the controller used to operate as a rotary position servo has a certain degree of freedom, which might be explored to achieve the performance required by each application. However, this cannot be done unless the effects of the controller changes are well known, thus also justifying the development of a model.

In the present paper, the dynamical model is built based on physical principles. Then, the constants are either directly obtained from the datasheets of the servo and of the DC motor used to build it, or are determined with data from some standard tests. After that, the model is enhanced to include quantization of the measurements, since an encoder is used to assess the angle of the load axis and saturation of the input voltage is also considered, given that the DC level of the feeding of the servo poses such a constraint. Finally, the model is validated against the frequency response and the step response data acquired from the actual servo. Thus, the contributions of this work are twofold: the formalization of a modeling procedure that can be applied to a class of servos and the development and validation of a mathematical model for the Dynamixel MX-28AT as one constructive example.

It is emphasized that, once the model is ob-

tained from physical principles, a variety of system identification techniques can be employed to obtain estimates of the model parameters (Ljung, 2017) from experimental data. For instance, algorithms that are optimal in a least-squares sense can be used to identify a transfer function from frequency response data (Drmac et al., 2014). On the other hand, identification of a continuous-time transfer function directly from sampled time-domain data require some care. Some alternatives, such as State-Variable Filters (SVF) and the Generalized Poisson Moment Functions (GPMF), can be employed to continuous-time parameter estimation (Garnier et al., 2003; Ljung, 2009). All of these methods are readily available in computer packages such as the System Identification Toolbox from Matlab (Mathworks, 2017). However, in the present work the model is obtained from data provided by the manufacturers of the DC motor and the servo, as these should be more representative of the range of DC motors and servos that are produced. On the contrary, if data from tests of a single servo were used, then the identified parameters might end up being very particular for that servo and not represent as well others. Therefore, in this work the data from the experiments of frequency and step responses of the servo are used only for validation of the model.

The remainder of the paper is divided as follows: the analytical model is obtained in Section 2, where the constants are also determined from the datasheet information. The model response and the experimental data are compared for validation in Section 3. Finally, concluding remarks are given in Section 4.

## 2 Mathematical model

In this section a model based on physical principles is developed for the Dynamixel MX-28AT position servo. For that purpose, the data from the data sheets of the DC motor used to build the servo and the one from the servo itself (including the gearbox) are employed.

The servo is built using an armature controlled Maxon DC motor model 214897 (Maxon Motors, 2015). The electric circuit equivalent of the motor is depicted in Fig. 1, where  $u$  is the input voltage at the terminals,  $e$  is the back electromotive force (EMF),  $i$  is the current,  $R$  is the resistance and  $L$  is the inductance.

The motor is assumed to have a torque constant  $K_t$  and a speed constant  $K_\omega$ . The angle of rotation of the motor shaft is  $\theta_m$  and its moment of inertia is  $J_m$ . Similarly, the angle of rotation in the load axis is  $\theta_l$  and its moment of inertia is  $J_l$ . Thus the equations involving the electrical

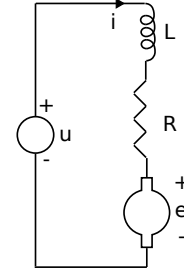


Figure 1: Electric circuit of the DC motor.

and mechanical parts are (Sen, 1997):

$$\tau_m = K_t i, \quad (1)$$

$$u = Ri + L \frac{di}{dt} + e, \quad (2)$$

$$e = \frac{\dot{\theta}_m}{K_\omega}, \quad (3)$$

$$J_m \ddot{\theta}_m = \tau_m - \frac{\tau_l}{N\eta} - \tau_{f,m}, \quad (4)$$

$$J_l \ddot{\theta}_l = \tau_l - \tau_{f,l}, \quad (5)$$

$$K_t = K_\omega^{-1}, \quad (6)$$

where  $\tau_m$  is the torque produced by the motor,  $\tau_l$  is the torque transmitted to the load,  $\tau_{f,m}$  and  $\tau_{f,l}$  are the friction torques at the motor and the the load shafts, respectively,  $N$  is the gear ratio of the gearbox and  $\eta$  is the gearbox efficiency factor. The moment of inertia of the load  $J_l$  varies according to the load connected to the servo. With exception of  $\tau_{f,m}$ ,  $\tau_{f,l}$  and  $\eta$ , the other parameters can be directly found in the datasheets. These three unknown parameters are determined in the following subsections.

### 2.1 Gearbox efficiency

Ideally, conservation of power in the gearbox would entail that  $P_m = P_l$ , where  $P_m$  is the power output of the motor (input to the gearbox) and  $P_l$  is the power transmitted to the load:

$$P_m = \dot{\theta}_m \tau_m = P_l = \dot{\theta}_l \tau_l. \quad (7)$$

Using the gear ratio  $N = 193$ , a relationship can be established between  $\dot{\theta}_m$  and  $\dot{\theta}_l$ :

$$\dot{\theta}_m = N \dot{\theta}_l. \quad (8)$$

Thus, combining (7) and (8):

$$\tau_m = \frac{\tau_l}{N}. \quad (9)$$

However, from the datasheets, the stall (when  $\dot{\theta} = 0$ ) torques  $\tau_{m,s}$  of the motor and  $\tau_{l,s}$  of the servo with an input voltage  $u = 12 V$  are:

$$\tau_{m,s} = 0.0155 Nm, \quad (10)$$

$$\tau_{l,s} = 2.5 Nm \quad (11)$$

These are incompatible with (9). Thus, it is assumed that some power is dissipated by the gearbox, resulting in a reduction of the actually transmitted torque. The proposal is to determine a gearbox efficiency factor  $\eta$  such that:

$$\tau_m = \frac{\tau_l}{N\eta}. \quad (12)$$

Using the stall torques, one can determine:

$$\eta = \frac{\tau_{l,s}}{N\tau_{m,s}} = \frac{2,5}{193 \times 0.0155} = 0.836. \quad (13)$$

It is assumed that this efficiency remains the same at all operating conditions, which is a standard assumption in electrical motor modeling.

## 2.2 Determining friction torques

The friction torques  $\tau_{f,m}$  in (4) and  $\tau_{f,l}$  in (5) are modeled as viscous friction:

$$\tau_{f,m} = b_m \dot{\theta}_m, \quad (14)$$

$$\tau_{f,l} = b_l \dot{\theta}_l. \quad (15)$$

The “no load” ( $NL$ ) condition of the motor means that  $\tau_{l,NL} = 0$  and the motor is at steady state, i. e.  $\dot{\theta}_{m,NL} = 0$ , in (4), therefore:

$$\tau_{m,NL} = \tau_{f,m,NL} = b_m \dot{\theta}_{m,NL} \rightarrow b_m = \frac{K_t i_{NL}}{\dot{\theta}_{m,NL}}. \quad (16)$$

The values  $i_{NL} = 0.0092$  A,  $\dot{\theta}_{m,NL} = 10600$  rpm and  $K_t = 0.0107$  Nm/A are found in the motor datasheet, entailing:

$$b_m = \frac{0.0107 \times 0.0092}{\frac{10600 \times 2\pi}{60}} = 8.87 \times 10^{-8} \text{ Nm.s}. \quad (17)$$

Applying a similar procedure using the “no load” ( $NL$ ) condition of the servo:

$$\tau_{l,NLs} = \tau_{f,l,NLs} = b_l \dot{\theta}_{l,NLs}. \quad (18)$$

Combining (3), (2) and (8), and using the value of the “no load” speed  $\dot{\theta}_{l,NLs} = 55$  rpm from the servo datasheet:

$$\begin{aligned} \tau_{m,NLs} &= K_t i_{NLs} = K_t \frac{u_{NLs} - \frac{N \times \dot{\theta}_{l,NLs}}{K_\omega}}{R} \\ &= 7.69 \times 10^{-5} \text{ Nm}, \end{aligned} \quad (19)$$

$$\begin{aligned} \tau_{f,m,NLs} &= b_m N \dot{\theta}_{l,NLs} \\ &= 9.87 \times 10^{-5} \text{ Nm}. \end{aligned} \quad (20)$$

These values are not compatible, as this would entail more friction torque than what is actually generated by the motor. It is advocated that the rounding of the data provided in the datasheets of the servo resulted in such an inconsistency. As a consequence, the proposal at this point is to simply disregard friction at the load shaft and make  $b_l = 0$ , simplifying the right hand side of (5) because  $\tau_{f,l} = 0$ .

## 2.3 Open-loop dynamical model

From (4) and (5):

$$J_l \ddot{\theta}_l = \tau_l = N\eta [\tau_m + \tau_{f,m} - J_m \ddot{\theta}_m], \quad (21)$$

and using (1) and (14):

$$J_l \ddot{\theta}_l = \tau_l = N\eta [K_t i - b_m \dot{\theta}_m - J_m \ddot{\theta}_m]. \quad (22)$$

Finally, using (8), a differential equation relating the load output angle  $\theta_l$  and the input current  $i$  can be found to be:

$$J_l \ddot{\theta}_l = \tau_l = N\eta [K_t i - b_m N \dot{\theta}_l - J_m \ddot{\theta}_m]. \quad (23)$$

To find the transfer function, it just remains to take the Laplace transform of (23) with null initial conditions, yielding:

$$\frac{\Theta_l(s)}{I(s)} = \frac{N\eta K_t}{(J_l + J_m N^2 \eta) s^2 + (b_m N^2 \eta) s}. \quad (24)$$

Considering now the electrical part, from (2) and (3):

$$u = Ri + L \frac{di}{dt} + \frac{\dot{\theta}_m}{K_\omega}. \quad (25)$$

Again taking the Laplace transform under the assumption of zero initial conditions:

$$U(s) = (R + Ls)I(s) + \frac{s\Theta_m(s)}{K_\omega}, \quad (26)$$

which, considering (8), yields:

$$I(s) = \frac{1}{R + Ls} U(s) - \frac{sN}{K_\omega(R + Ls)} \Theta_l(s). \quad (27)$$

Manipulating (24) and (27), one can determine the transfer function from the input voltage at the terminals  $U(s)$  to the output angle in the load shaft  $\Theta_l(s)$  as (28).

## 2.4 Closed-loop dynamical model

The controller that the manufacturer proposed for the MX-28AT is a Proportional-Integral-Derivative (PID), meaning that the input voltage is:

$$U(s) = \left( K_p + \frac{K_i}{s} + K_d s \right) [\Theta_r(s) - \Theta_l(s)], \quad (29)$$

where  $K_p$ ,  $K_i$  and  $K_d$  are the controller gains and  $\Theta_r(s)$  is the reference output angle.

Considering the servo input-output relation (28) and the controller transfer function (29), the closed-loop transfer function relating the commanded servo angle  $\Theta_r(s)$  and the measured one  $\Theta_l(s)$  is given in (30).

Simplifying this model is possible assuming that the electrical dynamics is much faster than the mechanical one, i. e., the time constant  $\frac{L}{R}$  is

$$\frac{\Theta_l(s)}{U(s)} = \frac{N\eta K_t}{s \left\{ L(J_l + J_m N^2 \eta) s^2 + [R(J_l + J_m N^2 \eta) + L b_m N^2 \eta] s + b_m N^2 \eta R + \frac{K_t N^2 \eta}{K_\omega} \right\}}. \quad (28)$$

$$\frac{\Theta_l(s)}{\Theta_r(s)} = \frac{N\eta K_t (K_d s^2 + K_p s + K_i)}{L(J_l + J_m N^2 \eta) s^4 + [R(J_l + J_m N^2 \eta) + L b_m N^2 \eta] s^3 + \left( b_m N^2 \eta R + \frac{K_t N^2 \eta}{K_\omega} + N\eta K_t K_d \right) s^2 + N\eta K_t K_p s + N\eta K_t K_i}. \quad (30)$$

much smaller than the mechanical time constants. Indeed, for the Dynamixel MX-28AT whose data are shown in Table 1, the poles of the open-loop transfer function (28) are 0, 161 and  $4.01 \times 10^4$ , where the last one is associated to the electrical dynamics, which can clearly be disregarded. This entails a lower-order closed-loop model given in (31).

Before documenting and discussing the results, it is important to make two remarks about the experimental setup:

**Remark 1** *The angle  $\theta_l$  is measured by an encoder, thus one needs to convert the measurements to radians in order to use the model (either (30) or (31)). Moreover, the reference to the servo must be converted from radians to counts, as the servo operates with this unit for the reference. The encoder resolution is  $\frac{4096}{2\pi}$  counts/rad.*

**Remark 2** *The output command of the controller  $u_c$  is given as a Pulse Width Modulated (PWM) signal. It was experimentally determined to be from 0 to 511 (0 meaning duty cycle of 0% of the applied voltage and 511 meaning duty cycle of 100% of the applied voltage, with a linear correspondence in between). It is assumed that the PWM frequency is high enough so that the effect perceived by the DC motor is an average voltage  $u = \frac{V_s}{511} u_c$  [V], where  $V_s$  is the voltage of the regulated current source feeding the servo.*

Due to remarks 1 and 2, a consequence is that the controller embedded in the servo operates as

$$U_c(s) = \left( K_p^c + \frac{K_i^c}{s} + K_d^c s \right) [\Theta_r^c(s) - \Theta_l^c(s)], \quad (32)$$

which is similar to (29), with the appropriate units:  $\Theta_r^c$  and  $\Theta_l^c$  given in *counts* and  $u_c$  given as a PWM value in the range specified in remark 2, therefore  $K_\bullet = K_\bullet^c \frac{2048 V_s}{511 \pi}$ , where  $\bullet = p, i, d$ .

Moreover, still considering remarks 1 and 2, two nonlinear phenomena are included in the model, namely: quantization of the angle measurements and saturation of the input voltage into the interval  $[-V_s, +V_s]$  V.

The values of the parameters for determining the transfer function can be found in Table 1, where the gains of the controller are determined from the default values from the manufacturer labeled as  $P$ ,  $I$  and  $D$  in the datasheet. The gains

Table 1: Parameters to determine the MX-28AT model.

Parameter		Value
Resistance	$R$	$8.3 \Omega$
Inductance	$L$	$2.03 \times 10^{-3} H$
Gear ratio	$N$	193
Gear efficiency	$\eta$	0.836
Speed constant	$K_\omega$	$93.1 rad/V$
Torque constant	$K_t$	$0.0107 Nm/A$
Inertia	$J_m$	$8.68 \times 10^{-8} kgm^2$
Friction	$b_m$	$8.87 \times 10^{-8} Nms$
Prop. gain	$K_p^c$	$P/8 = 4$
Int. gain	$K_i^c$	$1000I/2048 = 0$
Der. gain	$K_d^c$	$4D/1000 = 0$

that can be actually set in the servo are  $P$ ,  $I$  and  $D$ , so the conversion factors in Table 1 must be considered.

### 3 Experimental validation

To validate the proposed model, two kinds of experiments were performed with the MX-28AT fed from a regulated current source set up to provide  $V_s = 12 V$  and without any load  $J_l = 0$ : frequency response and step response. The results are shown in the present section.

The control of the servo was performed using a OpenCM 9.0.4 (ROBOTIS, 2010b) board from ROBOTIS using a baud rate of  $1Mbps$  and the reading of the servo positions and writing of a reference value was performed at every  $T_s = 0.005 s$ . The simulation model used for validation may be found as open-source software at [https://bitbucket.org/mmaximo/mx28\\_modeling](https://bitbucket.org/mmaximo/mx28_modeling).

#### 3.1 Frequency response

For the frequency response, sinusoidal inputs with varying frequency were used as reference inputs. In particular, knowledge of the theoretical frequency response from (30) is useful to determine a meaningful range of frequencies for the sinusoidal inputs. From the magnitude frequency response in Fig. 2, it can be seen that the gain is less than  $-14 dB$  for frequencies higher than  $128 rad/s$ , which is already a considerable attenuation. Therefore, the frequencies chosen for the frequency response experiment were no higher

$$\frac{\Theta_l(s)}{\Theta_r(s)} = \frac{N\eta K_t (K_d s^2 + K_p s + K_i)}{R(J_l + J_m N^2 \eta) s^3 + \left( b_m N^2 \eta R + \frac{K_t N^2 \eta}{K_\omega} + N\eta K_t K_d \right) s^2 + N\eta K_t K_p s + N\eta K_t K_i} \quad (31)$$

than 128 *rad/s*. In fact, the chosen frequencies grew in octaves between  $\omega_0 = 1$  *rad/s* and  $\omega_7 = 128$  *rad/s*, i. e.,  $\omega_i = 2^i$  *rad/s*,  $i \in \{0, 1, 2, \dots, 7\}$ . As for the amplitudes of the sinusoidal inputs, they were 400 *counts* peak-to-peak for frequencies between 1 *rad/s* and 16 *rad/s* and 200 *counts* peak-to-peak for frequencies ranging from 32 *rad/s* to 128 *rad/s*, to avoid saturation of the input voltage.

The model and experimental frequency responses can be seen in Figs. 2 and 3. It can be noticed that up until  $\omega_5 = 32$  *rad/s* the gain and phase both agree very well between the frequency responses of the model and the servo. The gain actually remains acceptable up until  $\omega_7 = 128$  *rad/s*, but from  $\omega_6 = 64$  [*rad/s*] to  $\omega_7 = 128$  [*rad/s*] the phase error is about  $25^\circ$ , which is already considerable for control applications. This could partially be explained by the readings of the data for recording purposes being performed at every  $T_s = 0.005$  *s*, which starts to represent a considerable delay in these frequencies.

Thus, from these results, it can be noticed that if one operates with input reference signals with a bandwidth of about 32 *rad/s*, the proposed model can be used to predict the actual response of the MX-28AT with reasonable fidelity. This is actually not very limiting for the normal uses of the servo such as in humanoid robots (Kajita et al., 2003; Maximo and Ribeiro, 2016).

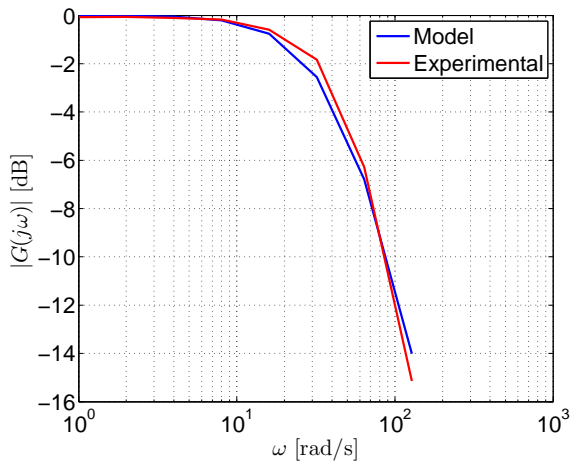


Figure 2: Magnitude frequency response.

### 3.2 Step response

The servo was started at three different angles  $\theta_{l,1}(0) = 100$  *counts*  $\approx 0.1534$  *rad*,  $\theta_{l,2}(0) = 200$  *counts*  $\approx 0.3068$  *rad* and  $\theta_{l,3}(0) = 400$  *counts*  $\approx 0.6136$  *rad*. To avoid angles out of

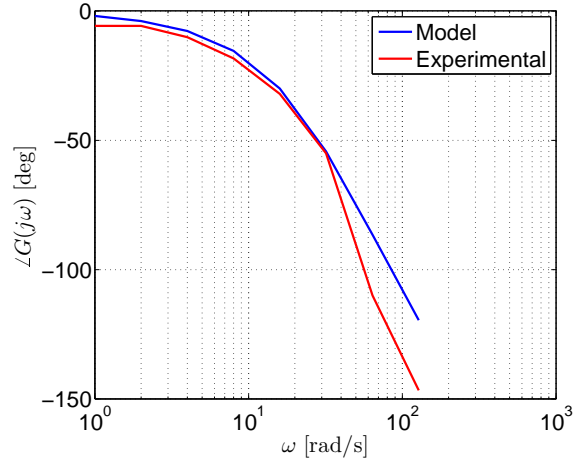


Figure 3: Phase frequency response.

the encoder range, the reference in each case was  $\theta_{r,i} = -(\theta_{l,i}(0) - 5)$  *counts*, meaning that the servo commanded position was initially 5 *counts*  $\approx 0.0077$  [*rad*] during 1 *s*, then it returned to  $\theta_r = 0$ .

Even with  $K_i = 0$ , the open-loop transfer function in (28) is of type 1, thus it is expected that there is no steady state error to a step input. From Fig. 4(a), the simulation results agree with this both for the linear and nonlinear models, however a small steady state error can be observed from the experimental data (the error oscillates between 1 and 2 encoder *counts*, i. e., at most 0.0031 *rad*). This could be attributed to dry friction, which is not present in the models (recall that the nonlinear phenomena considered in the model are only saturation of the voltage  $u$  and quantization of the measured angle  $\theta_l$ ). Therefore, one possible improvement of having a reasonable model of the servo is to choose  $K_i \neq 0$  so as to compensate this effect, but being able to account for the changes in the closed-loop pole locations. As observed, the steady state error was between 1 and 2 encoder *counts*, therefore one can use (32) to estimate the value of the dry friction torque. Since there is only a proportional control gain in this experiment:

$$U_c(s) = K_p^c [\Theta_r^c(s) - \Theta_l^c(s)]. \quad (33)$$

In steady state with an error of 2 *counts* and using  $K_p^c = 4$  from Table 1:

$$u_{c_{ss}} = 8. \quad (34)$$

From Remark 2, it means a duty cycle of  $8/511 = 0.0157$  of the source voltage, yielding an equivalent voltage of  $u_{ss} = \frac{V_s}{511} u_{c_{ss}} = 0.188$  [*V*]. Now admitting that the  $\dot{\theta}_{s_{ss}} = 0$  in (3) (recall that

the servo has already stopped in steady state in Fig. 4(a)), it follows from (2) that  $i_{ss} = u_{ss}/R = 0.0226 [A]$ . Using (1) with the steady state current  $i_{ss}$ , the motor torque is determined to be:

$$\tau_{m_{ss}} = K_t i_{ss} = 2.422 \times 10^{-4} [Nm]. \quad (35)$$

One can therefore argue that this motor torque is not enough to move the motor axis, therefore the static friction torque must be equal to that amount. This imposes a lower limit on the static dry friction (using a Coulomb model (Stribeck, 1902)). On the other hand, an upper limit can be found by noticing that the error is less than 3 *counts*. Repeating the calculations above, an error of 3 *counts* would entail a motor torque

$$\tau_{m_{ss}} = K_t i_{ss} = 3.633 \times 10^{-4} [Nm]. \quad (36)$$

Since this error never occurs in Fig. 4(a), this torque must be greater than the maximal value of the Coulomb dry friction torque. Thus, static friction referred to the motor axis is known to be  $\tau_{m_{st}} \in (2.422 \times 10^{-4}, 3.633 \times 10^{-4}) [Nm]$ . Since the effect of this dry static friction is minor (resulting in an error of 1 or 2 *counts*), disregarding it in the model does not affect the response severely. During the transient regime, the calculated viscous friction was assumed to be the only friction source, therefore all the friction phenomena are represented in this coefficient  $b_m$ , which is enough to allow a very precise matching between the responses from the servo and from the models, as seen in Fig. 4(a).

To observe the nonlinear phenomena more accurately, the results with larger reference changes can be seen in Figs. 4(b) and 4(c), for references  $\theta_{r_2} = -195 \text{ counts}$  and  $\theta_{r_3} = -395 \text{ counts}$ , respectively. The hypothesized dry friction being a nonlinear phenomenon, its effect should not behave linearly with the change on the reference input. It is indeed what can be observed comparing the steady state errors in Figs. 4(a), 4(b) and 4(c), where it can be noticed that the steady state error becomes less and less relevant with each increase in the reference amplitude, until it is barely visible in Fig. 4(c).

On the other hand, the effect of voltage saturation grows with the reference amplitude. With an amplitude of 95 *counts* in Fig. 4(a), the linear and nonlinear models responses are very similar and both agree well with the experiment. As the amplitude is increased to 195 *counts* a very subtle difference between the responses of the linear and nonlinear models appears as shown in Fig. 4(b). However, with the amplitude of 395 *counts* of the reference, it can be observed in Fig. 4(c) that there is a great mismatch between the simulation results of both models. Moreover, the response of the nonlinear model remains very close to the data from the servo, thus indicating that the saturation of the voltage is indeed the cause for a

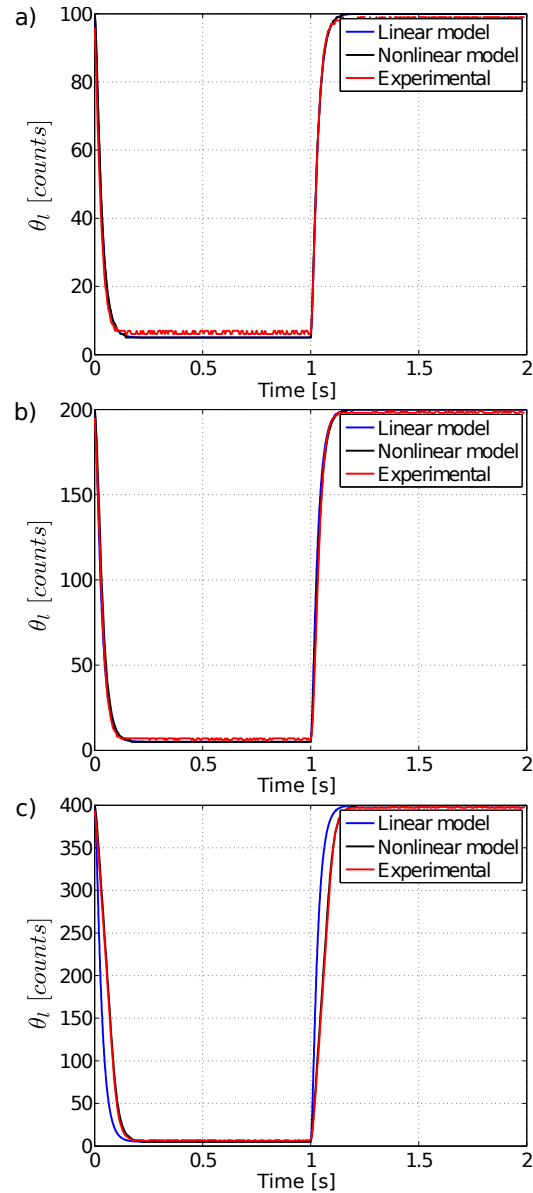


Figure 4: MX-28AT steps responses to inputs of (a)  $\theta_{r_1} = 95 \text{ counts}$ , (b)  $\theta_{r_2} = -195 \text{ counts}$ , and (c)  $\theta_{r_3} = -395 \text{ counts}$ .

poor prediction with the linear model. To perceive more clearly the outcomes of the saturation, the voltages resulting from the controller after saturation in the nonlinear simulation can be seen in Fig. 5, where it can be confirmed that the greater the reference, the larger the time that the voltage remains saturated.

#### 4 Conclusion

A model based mostly on physical principles and with usage of the data available from the datasheets was developed for the servo MX-28AT, with exception from the gain to convert from the PWM command to *volts*, which had to be determined through experimental observation. This analytical model was validated by two experi-

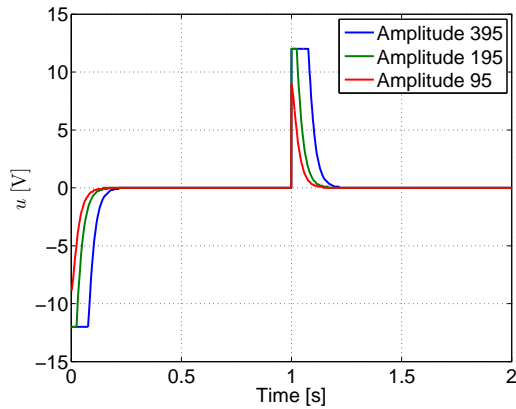


Figure 5: Simulated values of the voltages applied by the controller for the three reference amplitudes.

ments: frequency response and step response, showing good agreement with the experimental data. The availability of an adequate model opens many possibilities, such as high fidelity simulations of mechanisms that involve the servo as actuator and also redesign of the PID controller.

### Acknowledgments

The authors acknowledge the support of the São Paulo Research Foundation – FAPESP (grant 2016/03647-3). Carlos Ribeiro thanks CNPq for the research fellowship 303738/2013-8.

### References

- Drmac, Z., Gugercin, S. and Beattie, C. (2014). Quadrature-based vector fitting for discretized h2 approximation., *SIAM Journal on Scientific Computing* **37**(2): A625–A652.
- Garnier, H., Mensler, M. and Richard, A. (2003). Continuous-time model identification from sampled data: Implementation issues and performance evaluation, *International Journal of Control* **76**(13): 1337–1357.
- Gouaillier, D., Hugel, V., Blazevic, P., Kilner, C., Monceaux, J., Lafourcade, P., Marnier, B., Serre, J. and Maisonnier, B. (2009). Mechatronic Design of Nao Humanoid, *Proc. IEEE International Conference on Robotics and Automation (IROS)*, Kobe, Japan, pp. 769 – 774.
- Ha, I., Tamura, Y., Asama, H., Han, J. and .Hong, D. W. (2011). Development of Open Humanoid Platform Darwin-OP, *Proc. SICE Annual Conference*, Tokyo, Japan, pp. 2178–2181.
- Kajita, S., Kanehiro, F., Kaneko, K., Fujiwara, K., Harada, K., Yokoi, K. and Hirukawa,

H. (2003). Biped Walking Pattern Generation by using Preview Control of Zero-Moment Point, *Proc. International Conference on Robotics and Automation*, Taipei, Taiwan, pp. 14 – 19.

- Ljung, L. (2009). Experiments with identification of continuous-time models, *Proc. 15th IFAC Symposium on System Identification*, Vol. 42, Saint-Malo, France, pp. 1175–1180.
- Ljung, L. (2017). *Wiley Encyclopedia of Electrical and Electronics Engineering*, John Wiley & Sons, chapter System Identification, pp. 1–19.
- Mathworks (2017). System identification toolbox. Accessed in August 7th 2017. <https://www.mathworks.com/help/ident/index.html>
- Maximo, M. R. O. A. and Ribeiro, C. H. C. (2016). Omnidirectional ZMP-Based Humanoid Walking Engine, *Proc. 2016 Congresso Brasileiro de Automática (CBA)*, Vitória, Brazil.
- Maxon Motors (2015). *Maxon DC brushed motors: RE-max datasheet*, Maxon Motors.
- ROBOTIS (2010a). Robotis e-manual v1.29.00. Accessed April 24th 2017. [http://support.robotis.com/en/product/actuator/dynamixel/mx\\_series/mx-28.htm](http://support.robotis.com/en/product/actuator/dynamixel/mx_series/mx-28.htm)
- ROBOTIS (2010b). Robotis e-manual v1.30.00. Accessed 24th April 2017. [http://support.robotis.com/en/software/robotis\\_opencm\\_main.htm](http://support.robotis.com/en/software/robotis_opencm_main.htm)
- Sen, P. C. (1997). *Principles of Electric Machines and Power Electronics*, 2nd edn, John Wiley & Sons, New Jersey.
- Stribeck, R. (1902). Die wesentlichen eigenschaften der gleit - und rollenlager - the key qualities of sliding and roller bearings, *Zeitschrift des Vereines Seutscher Ingenieure* **46**(38-39): 1342–1348(38), 1432–1437(39).
- Wensing, P. M., Wang, A., Seok, S., Otten, D., Lang, J. and Kim, S. (2017). Proprioceptive Actuator Design in the MIT Cheetah: impact mitigation and high-bandwidth physical interaction for dynamic legged robots, *IEEE TRANSACTIONS ON ROBOTICS* **Preprint**: 1 – 14.
- Zhao, Y., Paine, N., Kim, K. S. and Sentis, L. (2015). Stability and Performance Limits of Latency-prone Distributed Feedback Controllers, *IEEE TRANSACTIONS ON INDUSTRIAL ELECTRONICS* **62**(11): 7151 – 7162.